Orientational properties of C_{70} and C_{80} fullerenes in carbon nanotubes

B. Verberck

Department of Physics, University of Antwerp, Groenenborgerlaan 171, 2020 Antwerpen, Belgium

(Received 28 October 2010; revised manuscript received 6 December 2010; published 20 January 2011)

We present energy calculations of a C_{80} molecule with D_{5d} symmetry encapsulated in a carbon nanotube. The approximation of a continuous tube rather than a rolled-up graphene sheet, justified by comparison with atomistic calculations, allows an expansion of the energy field into symmetry-adapted rotator functions. For a given tube radius R, we observe a strong dependence of the interaction energy on the molecular tilt angle and on the molecule's lateral position in the tube. We observe a transition from on-axis lying orientations to tilted orientations at $R_1 \approx 6.95$ Å and a subsequent transition to standing orientations at $R_2 \approx 7.6$ Å. For tube radii larger than $R_3 \approx 8.0$ Å, the molecule starts to occupy off-axis positions and assumes a lying orientation. Results are compared to the case of C_{70} molecules, with D_{5h} symmetry. Our findings are consistent with recent high-resolution transmission electron microscopy measurements and are relevant for the design of new materials with tunable electronic properties.

DOI: 10.1103/PhysRevB.83.045405 PACS number(s): 81.05.U−

I. INTRODUCTION

Since their discovery more than ten years ago, fullerene nanopeapods—single-walled carbon nanotubes (SWCNTs) filled with fullerene molecules—have been the subject of extensive experimental and theoretical research, and have opened a new direction in the field of one-dimensionally confined systems. C_{60}@SWCNT peapods were discovered first,[1] but various other fullerenes, C_n, have been inserted in nanotubes as well, e.g., with $n = 70$,[2,3] $n = 76$, $n = 78$, $n = 80$,[3,4] and so on. For reviews on fullerene (and other) peapod research, we refer to Refs. 5–8.

An interesting structural aspect of chains of encapsulated carbon cage molecules is their orientational behavior. In general, the interaction energy between a fullerene molecule and a surrounding nanotube depends on the molecule's degrees of freedom, and on the nanotube's structure. However, we have shown that for C_{60} and C_{70} molecules, the nanotube's actual honeycomb structure of carbon bonds does not have much influence on the optimal molecular configuration, and that it is justified to approximate the SWCNT as a continuous cylindrical carbon distribution.[9–11] Instead, the precise atomic structure of the fullerene determines its arrangement in the nanotube. For C_{60} peapods, three different optimal molecular orientations are obtained for tube radii R in the range 6.5–8.5 Å.[9,11–13] While these distinct orientations are difficult to observe directly because of the almost spherical shape of a C_{60} molecule, which has I_h symmetry (Fig. 1, left) recent neutron scattering experiments have been interpreted in terms of molecular orientational freezing consistent with the predicted potential energy landscapes.[14] The effect of radius-dependent lowest-energy molecular orientations is more pronounced for C_{70} peapods, because of the ellipsoidal shape of a C_{70} molecule, with D_{5h} symmetry (Fig. 1, middle). Indeed, for small tube radii, molecules adopt a lying orientation (long molecular axis parallel to the tube's long axis), and their centers of mass are further apart than for larger tube radii, where molecules orient with their long axis perpendicular to the tube's long axis (standing orientation). These two molecular orientations, implying different intermolecular distances, were observed first indirectly by means of electron diffraction (ED),[3] and later directly by means of high-resolution transmission electron microscopy (HRTEM).[15,16] Static energy calculations[10] predict lying orientations below $R = 6.93$ Å and standing orientations above $R = 7.18$ Å with respective intermolecular distances of $a = 11.0$ Å and $a = 9.8$ Å and are confirmed by ED (Ref. 3) and x-ray scattering experiments.[17]

While the notion of different orientations—and concomitant different intermolecular spacings—of C_{70} molecules enclosed in a CNT is well established by now, the practical importance of radius-dependent molecular ordering has only very recently been demonstrated: photoluminescence measurements on C_{70}@SWCNT peapods have revealed the influence of the molecular orientations on the peapods' electronic properties.[18] In parallel, progress is being made on the synthesis and characterization of novel fullerene peapod systems. In particular, a recent aberration-corrected electron microscopy study reaching atomic resolution clearly showed molecular reorientations of tubular C_{80} fullerenes with D_{5d} symmetry (Fig. 1, right) encapsulated in SWCNTs.[19] A transition from lying to standing orientations as observed for C_{70} peapods is expected for D_{5d} C_{80}@SWCNT; it is one of the goals of the present paper to obtain precise values for the transition radii.

Realizing the increasing interest—from the point of view of possible applications—of fullerene peapod systems and considering the continuing research on their synthesis, we set out to investigate the D_{5d} C_{80}@SWCNT peapod system, focusing on the dependence of the molecular orientation on the tube radius. Apart from providing insight into the possible optimal configurations for the specific case of D_{5d} C_{80} peapods, our study complements earlier work and allows us to compare spherical, ellipsoidal, and tubular encapsulated fullerene molecules.

Apart from the difference in size, the C_{70} and C_{80} fullerenes considered here have different point group symmetries—D_{5h} and D_{5d}, respectively.[20] Both exhibit a fivefold rotation axis; D_{5h} symmetry features a mirror plane perpendicular to the fivefold axis while the D_{5d} point group has an inversion center. The different symmetries of C_{70} and C_{80} can be appreciated from the bond maps shown in Fig. 2. They are obtained

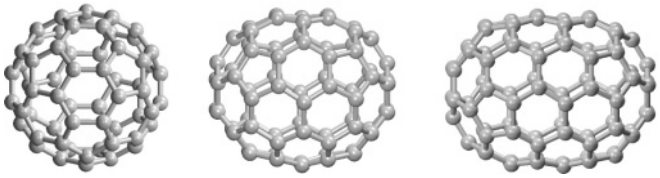

FIG. 1. Fullerene molecules display different symmetries: (left) C_{60}, I_h symmetry; (middle) C_{70}, D_{5h} symmetry; (right) C_{80}, D_{5d} symmetry.

by first aligning the molecule's long axis to the z axis, transforming the bonds—parametrized as three-dimensional $(x(t),y(t),z(t))$ straight-line fragments—into two-dimensional $(\phi(t),\theta(t))$ paths.[23] Plotting these $(\phi(t),\theta(t))$ curves then results in Mercator maps[24] nicely showing the typical fullerene structures consisting of pentagons and hexagons. A color coding has been superimposed on the bond maps in Fig. 2 to highlight the differences in symmetry. For both D_{5h} and D_{5d}, the fivefold symmetry axis manifests itself as $360^\circ/5$ periodicity in ϕ. The mirror plane perpendicular to the z axis, for D_{5h}, is observed as invariance upon mirroring the (ϕ,θ) map about the $\theta = 90^\circ$ straight line (Fig. 2, top). For D_{5d}, the inversion operation is transformed into a glide-mirror operation in (ϕ,θ) coordinate space: mirroring about the $\theta = 90^\circ$ straight line and shifting horizontally (constant θ) from ϕ to $\phi + 180^\circ$ (Fig. 2, bottom). The five mirror planes through the z axis, present for both symmetries, are converted into mirror lines at $\phi = 0^\circ$, 36°, 72°, ... Note that for D_{5d}, the z axis is not only a fivefold rotation axis but also a tenfold inversion axis.

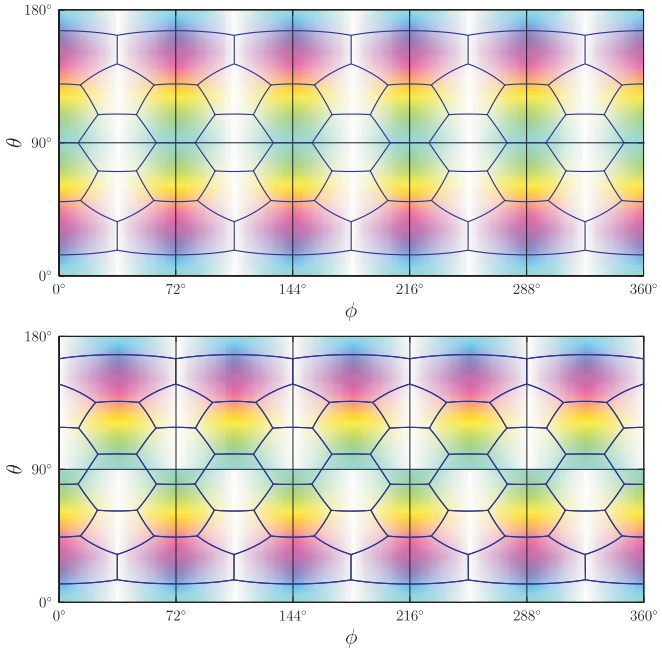

FIG. 2. (Color online) Bond maps of (top) C_{70} and (bottom) C_{80} molecules. Color maps displaying (top) D_{5h} and (bottom) D_{5d} symmetry have been superimposed to emphasize the differences between both point groups.

II. NANOTUBE FIELD

A. Atomistic formulation

We consider a single C_{80} molecule encapsulated in a SWCNT; the molecule's center of mass lies on the nanotube's long axis. For describing the molecule's orientation, we employ Bradley and Cracknell's Euler angle convention,[25] where the three Euler rotations are (i) an initial rotation over $0 \leqslant \alpha < 2\pi$ about the z axis, followed by (ii) a rotation over $0 \leqslant \beta \leqslant \pi$ about the y axis, followed by (iii) a final rotation over $0 \leqslant \gamma < 2\pi$ about the z axis. The x, y, and z axes are kept fixed. The z axis of the Cartesian system of axes (x,y,z) is chosen to coincide with the tube's long axis. As starting orientation, $\alpha = \beta = \gamma = 0$, we take the orientation where the C_{80} molecule's fivefold axis coincides with the tube's long axis and one of the two "pentagons" perpendicular to the z axis has one atom with coordinates $(x > 0, y = 0, z > 0)$—we call this orientation the "standard orientation" (Fig. 3). For the D_{5d} C_{80} molecule's atomic coordinates we slightly adjusted the coordinates of Ref. 26 so that D_{5d} symmetry was indeed present.

A SWCNT with chiral indices (n,m) is obtained by rolling up a graphene sheet with basis vectors $\vec{a}_1 = a\vec{e}_X$ and $\vec{a}_2 = a\frac{1}{2}\vec{e}_X + a\frac{3}{2}\vec{e}_Y$, where $\vec{e}_X$ and $\vec{e}_Y$ are planar Cartesian basis vectors, along the vector $\vec{C}(n,m) = n\vec{a}_1 + m\vec{a}_2$.[27,28] The distance $a = 2.49$ Å is related to the C-C bond length d_{CC} in graphene: $d_{CC} = a/\sqrt{3} = 1.44$ Å.[27,28] We position the resulting tube so that the C atom originally (before rolling up) at $0\vec{e}_X + 0\vec{e}_Y$ lies in the (x,y) plane with x coordinate 0 and y coordinate R—the tube's radius—and so that the cylinder containing the C atoms has its long axis coinciding with the z axis.

The foregoing settles the (x,y,z) coordinate system, the arrangement of the carbon nanotube, and the starting orientation of the C_{80} molecule. It also implicitly fixes the molecule's initial position along the tube axis. However, for an infinite nanotube, any position obtained by a shift ζ along the z axis should be treated on the same footing as the original one ($\zeta = 0$). Hence, the interaction energy of the C_{80} molecule generally depends on the four variables α, β, γ, and ζ, and on the tube indices n and m: $V_{\mathrm{NF}} \equiv V_{\mathrm{NF}}(\alpha,\beta,\gamma;\zeta;n,m)$. Here, the subscript "NF" stands for "nanotube field." Indeed, the

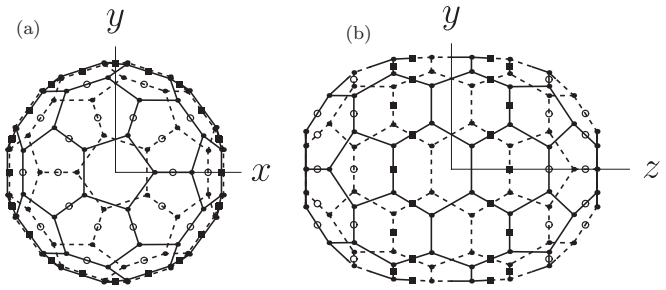

FIG. 3. A D_{5h} C_{80} molecule in the standard orientation: (a) projection onto the (x,y) plane, and (b) projection onto the (y,z) plane. In (a), bonds lying below the (x,y) plane ($x < 0$) are shown dashed, in (b), bonds lying below the (y,z) plane. Interaction centers are shown as dots (atoms), circles (D centers) and filled squares (I centers).

interaction energy can be interpreted as an energy field set up by the nanotube surrounding the C_{80} molecule.

The interaction between the C_{70} molecule and the nanotube is of van der Waals type—HRTEM observations of peapods reveal the motion of the fullerene molecules along the tube axis and rule out chemical bonds.[3,19] The most straightforward way to describe the interaction of the molecule with the nanotube is to take the atoms of the molecule as point centers which interact with the atoms of the nanotube. Assuming atom-atom pair interactions, the total interaction energy reads

$$V_{\mathrm{NF}} = \sum_{\Lambda_a} \sum_{\tau} v^{\mathrm{a}}\big(|\vec{r}_{\tau} - \vec{r}_{\Lambda_a}|\big), \tag{2.1}$$

where $\Lambda_a = 1, \ldots, N_a = 80$, indexes the 80 C atoms of the molecule and τ the C atoms of the tube. In Eq. (2.1), $\vec{r}_{\tau}$ and $\vec{r}_{\Lambda_a}$ are the position vectors of atom τ of the nanotube and atom Λ_a of the molecule, respectively. The van der Waals pair potential v^{a} only depends on the interatomic distance $|\vec{r}_{\tau} - \vec{r}_{\Lambda_a}|$. As for the case of C_{70} molecules, we treat certain (midpoints of) bonds of the C_{80} molecule as point interaction centers (ICs) too. Each of the two C_{60}-like hemispheres ("caps") features 10 "D centers," while the regions next to the caps are populated with 30 "I centers"; see Fig. 3. We label the 20 D centers and the 30 I centers by the indices $\Lambda_D = 1, \ldots, N_D = 20$, and $\Lambda_I = 1, \ldots, N_I = 30$, respectively. The generalization of Eq. (2.1) then reads

$$V_{\mathrm{NF}} = \sum_{\mathrm{t=a,D,I}} \sum_{\Lambda_t=1}^{N_t} \sum_{\tau} v^{\mathrm{t}}\big(|\vec{r}_{\tau} - \vec{r}_{\Lambda_t}|\big), \tag{2.2}$$

with t indexing the type of IC of the C_{80} molecule. For the type-dependent pair interactions we use Born–Mayer–van der Waals potentials:

$$v^{\mathrm{t}}(r) = C_1^{\mathrm{t}} e^{-C_2^{\mathrm{t}} r} - \frac{B^{\mathrm{t}}}{r^6}. \tag{2.3}$$

Born–Mayer–van der Waals potentials have been successfully used for modeling intermolecular interactions in solid C_{60}: Launois *et al.*[29] have tested several potential models (including 12-6 Lennard-Jones potentials and potential models assuming point charges on the C_{60} cage) and found that the Born–Mayer–van der Waals model of Lamoen and Michel[30] fits diffuse x-ray diffraction data best. Later, a similar potential was used for modeling solid C_{70},[31] which was then in turn adapted to describe C_{70}-SWCNT interactions.[10] Here, we use the same set of potential constants as in Ref. 10.

Note that the CNT does not exhibit bond ICs, i.e., the 80 + 20 + 30 ICs of the C_{80} molecule only interact with the tube's C atoms. For actual numerical computation of the nanotube field V_{NF} via Eq. (2.2), the sum over tube atoms—with coordinates $\vec{r}_{\tau} = (x_{\tau}, y_{\tau}, z_{\tau})$—has to be restricted to atoms in a certain vicinity of the C_{80} molecule, realized by imposing the criterion

$$z_{\min} \leqslant z_{\tau} \leqslant z_{\max}, \tag{2.4}$$

with $z_{\min}$ and $z_{\max}$ cutoff values chosen to ensure convergence.

B. Continuous formulation

The nanotube field V_{NF} generally depends on six variables: α, β, γ, ζ, n, and m. The number of variables can be halved by neglecting the nanotube's discrete structure. Indeed, if one assumes a continuous distribution of carbon atoms on a cylinder, the indices n and m are replaced by the radius R, and furthermore, the translational coordinate ζ and one of the Euler angles become irrelevant. We distinguish this "smooth-tube" approach from the "discrete-tube" approach described in the preceding section by adding superscripts: $V_{\mathrm{NF}}^{\mathrm{smooth}} \equiv V_{\mathrm{NF}}(\beta,\gamma;R_{\mathrm{T}})$ and $V_{\mathrm{NF}}^{\mathrm{discrete}} \equiv V_{\mathrm{NF}}(\alpha,\beta,\gamma;\zeta;n,m)$. A continuum approximation for the nanotube in combination with an atomistic description for a fullerene molecule was first introduced in Ref. 12 for C_{60}@SWCNT peapods; its validity was tested in detail in Ref. 9. Later, it was applied and justified for C_{70}@SWCNT peapods as well.[10] Here we extend the approach to fullerene molecules with D_{5d} symmetry (we recall that the molecular point-group symmetries of C_{60} and C_{70} are I_h and D_{5h}, respectively).

The radius R of a tube with indices (n,m) reads $R = \frac{a}{2\pi}\sqrt{n^2+nm+m^2}$, and its surface density σ—common for all carbon nanotubes, i.e., radius independent—can be readily calculated to be $\sigma = \frac{4}{\sqrt{3}a^2} = 0.372\ \text{Å}^{-2}$. The nanotube field is then obtained as

$$V_{\mathrm{NF}}^{\mathrm{smooth}}(R) = \sigma R \sum_{\mathrm{t=a,D,I}} \sum_{\Lambda_t=1}^{N_t} \int_0^{2\pi} d\Phi \int_{-\infty}^{+\infty} dZ\ v^{\mathrm{t}}\big(|\vec{\rho} - \vec{r}_{\Lambda_t}|\big), \tag{2.5}$$

where $\vec{\rho}$ is the position vector of a point on the cylindrical tube ($\rho_x = R\cos\Phi$, $\rho_y = R\sin\Phi$, $\rho_z = Z$). Analogous to limiting the summation over tube atoms in Eq. (2.2) via criterion (2.4), the integral over Z in Eq. (2.5) needs to be limited to the finite interval $z_{\min} \leqslant Z \leqslant z_{\max}$.

It can be shown[10] that Eq. (2.5) can be elaborated into the following form:

$$V_{\mathrm{NF}}^{\mathrm{smooth}}(\beta,\gamma;R) = \sigma R \sum_{\mathrm{t}} \sum_{\lambda_t} \sum_{l=0,1,2,\ldots}^{\infty} w_l^{\mathrm{t}}(\lambda_t,R)\mathcal{U}_l^{\mathrm{t}}(\lambda_t;\beta,\gamma). \tag{2.6}$$

Here, the index λ_t refers to "layers" of ICs of type t (t = a,D,I): a layer groups ICs with the same $|z_{\Lambda_t}|$ value. The symmetry-adapted rotator functions (SARFs) $\mathcal{U}_l^{\mathrm{t}}(\lambda_t;\beta,\gamma)$ are linear combinations of spherical harmonics $Y_l^n(\beta,\gamma)$; they account for the symmetry of the molecule and of the nanotube:

$$\mathcal{U}_l^{\mathrm{t}}(\lambda_t;\beta,\gamma) = \sqrt{\frac{4\pi}{2l+1}} \sum_{n=-l}^{l} \alpha_l^{\mathrm{t},n}(\lambda_t) Y_l^n(\beta,\gamma). \tag{2.7}$$

More details on the expansion into SARFs, the expansion coefficients $w_l^{\mathrm{t}}(\lambda_t,R)$, and the molecular coefficients $\alpha_l^{\mathrm{t},n}(\lambda_t)$ are given in the Appendix.

The D_{5d} symmetry of the C_{80} molecule imposes the following selection rules on the multipole coefficients $\alpha_l^{\mathrm{t},n}(\lambda_t)$:

$$\alpha_l^{\mathrm{t},n}(\lambda_t) \neq 0 \ \text{ if } l \text{ even and } n = 0, \pm 5, \pm 10, \ldots, (D_{5d}). \tag{2.8}$$

This significantly limits the nonvanishing terms of the SARF expansion [Eq. (2.6)], the only occurring terms with $l \leqslant 12$ are $(l,m) = (0,0), (2,0), (4,0), (6,0), (6,5), (8,0), (8,5), (10,0),$

(10,5), (10,10), (12,0), (12,5), and (12,10). We recall the selection rule for C_{70} molecules,

$$\alpha_l^{t,n}(\lambda_t) \neq 0 \text{ if } l+n \text{ even and } n = 0, \pm 5, \pm 10, \ldots, (D_{5h}), \tag{2.9}$$

resulting in the following lowest-order terms: $(l,m) = (0,0)$, (2,0), (4,0), (5,5), (6,0), (7,5), (8,0), (9,5), (10,0), (10,10), (11,5), (12,0), and (12,10).

As has already been shown for C_{60} and C_{70} peapods and will become clear for C_{80} peapods below, a serious advantage of the SARF expansion is that a limited number of terms already gives extremely good convergence. We point out that expansion (2.6) provides a computationally efficient way of calculating V_{NF}^{smooth}—the gain in calculation speed, as compared to using Eq. (2.5) and explicitly performing coordinate transforms, is significant.

C. Results: Comparison of continuous and atomistic approaches

We have calculated the nanotube field for a C_{80} molecule, centrally positioned in a SWCNT, via both the atomistic and the continuum approaches [Eqs. (2.2) and (2.6), respectively], for a representative selection of tubes with radii in the range $6.0 \leqslant R < 12$ Å. As discussed above, the smooth-tube approach has the advantage of resulting in a nanotube field depending only on the Euler angles (β,γ) and the tube radius R. For a given tube radius, the nanotube field can therefore be visualized as a (β,γ) Mercator map. The discrete-tube approach on the other hand displays full (α,β,γ) and ζ dependence. However, we have shown previously that for C_{60} (Ref. 9) and C_{70} (Ref. 10) molecules, the nanotube field's α and ζ dependence is negligible compared to its variation with β and γ. We therefore put $\alpha = 0$ and $\zeta = 0$ for the atomistic calculations. For the z integrations, we have used the boundaries $-z_{min} = z_{max} = 50$ Å [see Eq. (2.4)].

In Fig. 4, the Mercator maps $V_{NF}^{discrete}(\alpha = 0,\beta,\gamma;\zeta = 0;n,m)$ and $V_{NF}^{smooth}(\beta,\gamma;R)$ are shown for a (10,10) tube ($R = 6.86$ Å). While small differences between the discrete and smooth approaches are discernible, the overall agreement is very good. The main difference between the two cases is the stronger variation with γ within the atomistic description. At $\beta = 90°$, the energy variation of $V_{NF}^{discrete}$ when varying γ is about 2.4×10^3 K $\times k_B$. This variation is small compared to the variation of V_{NF} with β, about 8.3×10^4 K $\times k_B$. The energy minimum lies at $\beta_{min} = 0°$, corresponding to a lying molecular orientation.

Comparison of $V_{NF}^{discrete}$ and V_{NF}^{smooth} for an (18,1) tube ($R = 7.34$ Å), Fig. 5, leads to similar observations: the discrete approach displays a more pronounced variation with γ than the smooth-tube approximation, but overall agreement of the energy values is satisfactory. (The global energy variation is 7.6×10^3 K $\times k_B$; the energy variation at the optimal β angle is 90 K $\times k_B$.) Interestingly, the energy minimum now lies at $\beta_{min} = 36°$, implying a tilted optimal molecular orientation.

A systematic comparison of discrete and smooth (β,γ) Mercator maps for several tubes shows that the agreement improves with increasing tube radius. Figure 6, showing energy plots for a (20,0) tube ($R = 7.93$ Å), is representative for radii larger than 7.5 Å, for which $V_{NF}^{discrete}$ and V_{NF}^{smooth} match very well. The γ dependence has become very weak, and the energy minimum lies at $\beta_{min} = 90°$, corresponding to a standing molecular orientation (the global energy variation is 6.6×10^3 K $\times k_B$; the energy variation at $\beta = 90°$ reaches only 30 K $\times k_B$.)

We can conclude that the smooth-tube approximation works very well, especially for tubes with $R > 7.5$ Å. We would like to stress the importance of this observation: as mentioned before, the computational gain when using SARFs is large: on one and the same machine, the computation of the expansion coefficients $\tilde{v}_l^t(R,\lambda_t)$ [Eq. (A3b)] for a given radius R, followed by the evaluation of $V_{NF}^{smooth}(\beta,\gamma;R)$ [Eq. (2.6)], took about

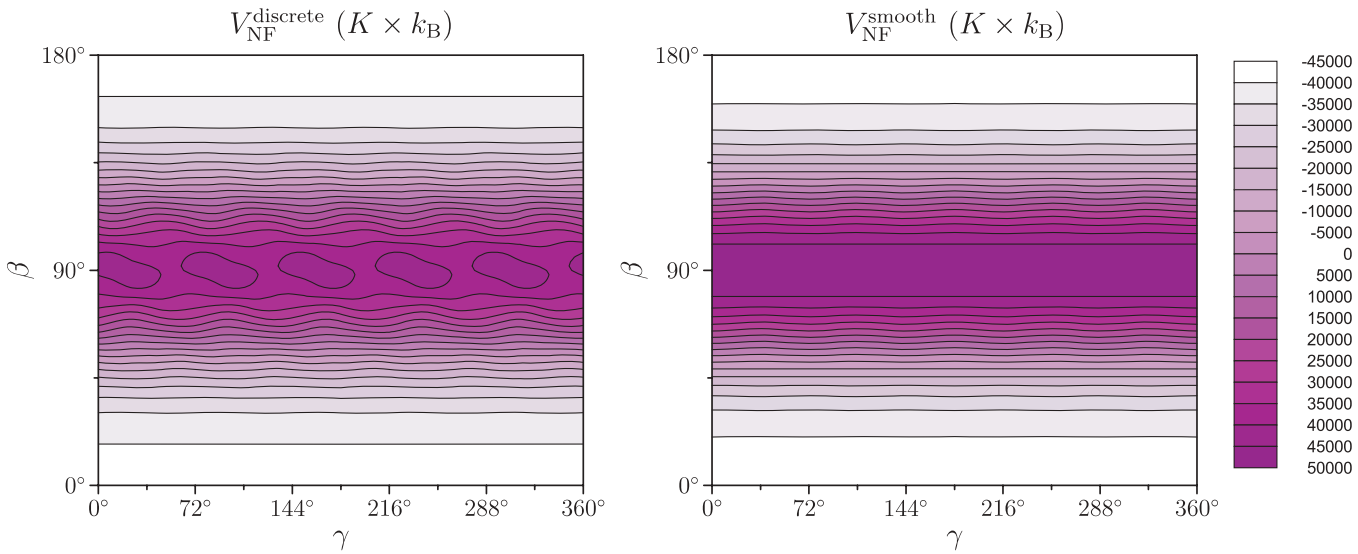

FIG. 4. (Color online) Nanotube field of a (10,10) nanotube experienced by a D_{5d} C_{80} molecule, obtained with the discrete (left) and smooth (right) approach.

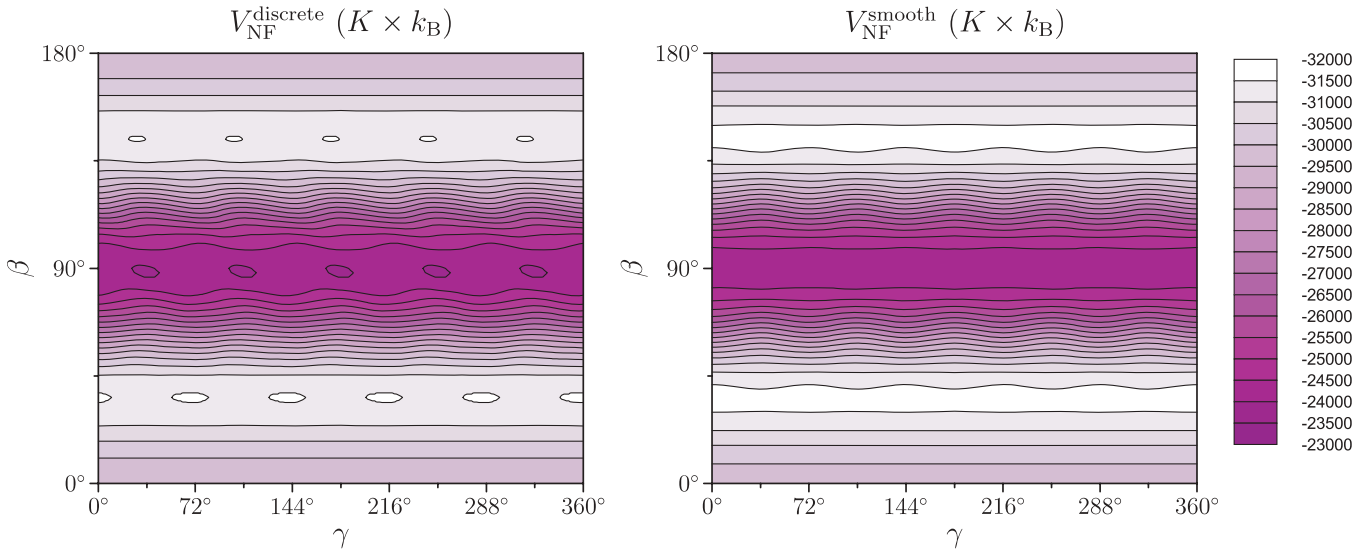

FIG. 5. (Color online) Nanotube field of an (18,1) nanotube experienced by a D_{5d} C_{80} molecule, obtained with the discrete (left) and smooth (right) approach.

a minute, while the calculation of $V_{\mathrm{NF}}^{\mathrm{direct}}(\alpha = 0,\beta,\gamma;\zeta = 0,n,m)$ [Eq. (2.2)] took more than one hour. The generally weak dependence of V_{NF} on γ means that an initial molecular rotation about the z axis over $-\gamma$ has almost no influence on the nanotube field. On the other hand, the subsequent rotation about the y axis over $-\beta$ has a high impact; the energy scale is completely determined by the C_{80} molecule's tilt angle β. The energy minimum's location evolves from $\beta_{\mathrm{min}} = 0°$ for small tubes to $\beta_{\mathrm{min}} = 90°$ for large tubes; we investigate this transition in more detail in the following section. Mathematically, the weak $V_{\mathrm{NF}}(\gamma)$ dependence can be traced to the selection rule for the $\alpha_l^{\mathrm{t},n}$ coefficients [Eq. (2.9)]. Indeed, only $n = 0$ coeffients—displaying no γ dependence—enter the leading terms ($l = 0,2,4$), an effect similar to the case of C_{70} molecules (D_{5h} symmetry) where nonvanishing γ-dependent terms start to occur only from $l = 10$ onward.[10]

The physical implication of the weak γ dependence is the ability to perform free rotations about the molecule's long axis down to extremely low temperatures. Within the smooth-tube approximation, for lying molecules, there is even no energy barrier to performing such spinning rotations. But even within the discrete approach, we find extremely small barriers ΔE_γ: for, e.g., the (10,10) tube (Fig. 4), $\Delta E_\gamma = 15\ \mathrm{K} \times k_{\mathrm{B}}$.

III. OPTIMAL MOLECULAR CONFIGURATION

A. On-axis positions

The minimum-energy angles β_{min} derived from the Mercator maps above suggest the following general, intuitively plausible, trend. For low tube radii, the optimal configuration is the lying orientation—molecular long axis parallel to the tube axis [Fig. 7(a)]. From a certain tube radius R_1 onward,

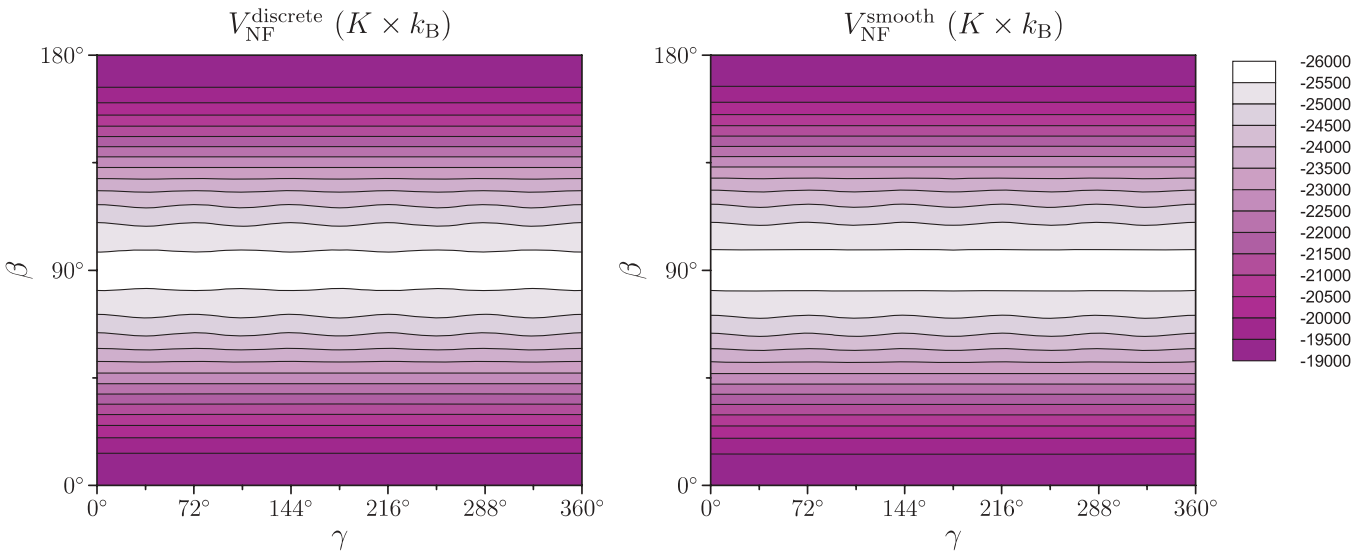

FIG. 6. (Color online) Nanotube field of a (20,0) nanotube experienced by a D_{5d} C_{80} molecule, obtained with the discrete (left) and smooth (right) approach.

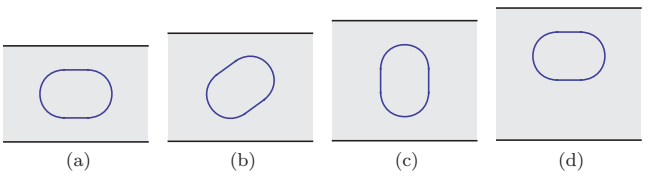

FIG. 7. (Color online) Schematic representation of on-axis lying (a), tilted (b), standing (c), and off-axis lying (d) D_{5d} C_{80} molecules.

the molecule starts to tilt away from the lying orientation [Fig. 7(b)]. For still larger tube radii, $R > R_2$, the standing orientation [Fig. 7(c)] is reached. In order to get an accurate estimate for the transition radius interval $R_1 < R < R_2$, we have calculated $V_{\mathrm{NF}}(\beta,\gamma;R)$ for the range $6.0 \leqslant R < 11.0$ Å with increments of 0.05 Å, and have extracted the optimal angle β_{min} for each case. The result is shown in Fig. 8(a), left part. We find that $R_1 \approx 6.95$ Å and $R_2 \approx 7.6$ Å. In Fig. 8(b), left part, we have plotted the $\beta_{\mathrm{min}}(R)$ dependence for a C_{70} molecule in a nanotube.[32] For C_{70}, the transition radius interval is considerably smaller ($6.95 \lesssim R \lesssim 7.15$ Å). This is obviously due to the longer shape of a C_{80} molecule, needing more space (larger tube radius) to develop a standing configuration.

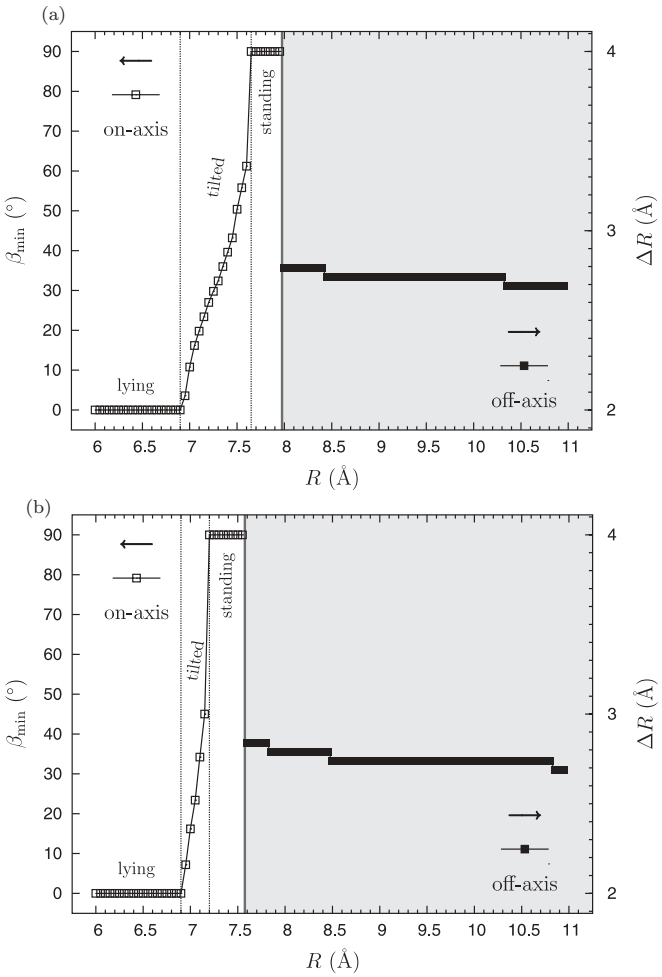

FIG. 8. Optimal tilt angle β_{min} (left ordinate) and off-axis displacement Δx(right ordinate) for (a) a C_{80} and (b) a C_{70} molecule in a SWCNT.

B. Off-axis positions

Up to now, we have assumed that a fullerene molecule in a nanotube has its center of mass on the tube axis (z axis). While this is a plausible assumption for small tube radii—the surrounding wall then repels the encapsulated molecule—it is expected that from a certain radius R_3 onward, it is more favorable for the molecule to "stick" to the nanotube wall and assume an off-axis position [Fig. 7(d)]. We have investigated this possibility by calculating the nanotube field for C_{80} molecules shifted over Δx along the x axis, for both lying ($\beta = 0°, \gamma = 0°$) and standing ($\beta = 90°, \gamma = 0°$) orientations, for the same range of tube radii as for the on-axis calculations ($6.0 \leqslant R < 11.0$ Å). Note that this requires direct integration; the SARF expansion as presented in Sec. II B cannot be applied because of the broken cylindrical symmetry. We then compared the resulting energy values with the on-axis energies, and found that from $R_3 \approx 8.0$ Å onward, lying off-axis configurations start to be more favorable than standing on-axis configurations. We introduce the quantity $\Delta R = R - (\Delta x + r_1)$, with $r_1 = 3.56$ Å half the length of the short axis of the C_{80} molecule (the radius of the molecule's central "tubular part"), and plot its dependence on R in the right part of Fig. 8(a); ΔR is the distance between the nanotube wall and the molecule's tubular part. We find values decreasing from $\Delta R = 2.8$ to 2.7 Å, smaller than the 3.4 Å observed in graphite and concentric double-walled CNTs (DWCNTs),[33] which can be explained by the contribution from the ICs farther away (e.g., on the caps) driving the molecule closer to the tube wall. Considering only the tubular part of the molecule (neglecting the caps), the different curvatures (r_1 and R) of the molecule and the surrounding tube also imply the molecule's being closer than 3.4 Å to the tube. This also explains the slight decrease of ΔR with increasing R.

A C_{70} molecule has a shorter cylindrical body than a C_{80} molecule. Therefore, a standing orientation cannot be maintained for radii larger than $R_3 \approx 7.6$ Å [Fig. 8(b), right part], and a lying off-axis configuration is more favorable. Note that in Ref. 10 it was erroneously assumed that from a certain radius onward, a standing off-axis arrangement can be optimal, because the lying off-axis calculation was not performed for larger tube radii. We can therefore conclude that for both C_{70} and C_{80} molecules, a lying configuration is always preferred to a standing configuration.

Aberration-corrected electron microscopy experiments allow one, by comparing experimentally obtained HRTEM images with simulations, to precisely determine both the position and orientation of D_{5d} C_{80} molecules in a SWCNT .[19] In particular, images of C_{80} molecules in an (18,1) nanotube [Fig. 1(d) in Ref. 19] show an on-axis position and a tilt of 30°. Our calculated value of $\beta_{\mathrm{min}} \approx 36°$ for an (18,1) peapod (see Fig. 5) is consistent with the experimentally observed tilt angle if one takes temperature fluctuations into account.

IV. DISCUSSION AND CONCLUSIONS

Our potential energy calculations for a D_{5d} C_{80} molecule in a carbon nanotube show that, when the molecule is positioned on the tube's long axis, the molecule's optimal tilt angle β_{min} changes from 0° (lying) to 90° (standing) when the tube radius R is increased [Figs. 7(a)–7(c)]. Obviously, such

a transition must take place because of simple energetic arguments: repulsion at short distances, attraction at larger distances. The goal of the numerical calculations presented here is to provide actual numbers marking different regimes: the transition from lying to standing takes place in the interval $R_1 \approx 6.95$ Å $\leqslant R \leqslant R_2 \approx 7.6$ Å. This range is considerably broader than for a C_{70} molecule in a nanotube ($R_1 \approx 6.95$ Å, $R_2 \approx 7.15$ Å), and has important implications for peapod fabrication and their possible use for electronic applications. Production of nanotubes, and hence peapods, with given tube indices (n,m), or even with a narrow radius distribution around a given mean tube radius $\overline{R}$, continues to be a challenging problem in present-day carbon science. Therefore, a larger radius separation between lying and standing regimes certainly is an advantage for the production of lying-only or standing-only peapods. We stress the importance of this observation in view of recent photoluminescence measurements on C_{70}@SWCNT samples revealing dependence on the C_{70} molecules' orientations;[18] a similar dependence is expected for C_{80} peapods. We point out that in a real peapod, molecules interact not only with the nanotube, but also with neighboring molecules. However, a comparison of the magnitudes of both types of interaction energy shows that the molecular orientations (tilt angles) and positions (on or off axis) are hardly influenced by the intermolecular interactions.[9,10] It follows that the electronic properties of a SWCNT can be tuned not only by inserting different molecules (C_{60}, C_{70} or C_{80} fullerenes), but also by controlling the molecules' orientations. They depend mainly on the SWCNT's radius, but are also influenced by temperature. Indeed, a recent Monte Carlo simulation study of C_{70} peapods shows that molecules in standing orientations start to perform quasifree three-dimensional rotations when the temperature is increased up to 1000 K.[34] Thermal sensors are conceivable devices exploiting the dependence of the photoluminescence spectrum of a fullerene peapod on the orientations of its molecular constituents.

Apart from the possibility of electronic applications, another reason why fullerene nanotubes are interesting materials is their thermal behavior: high-temperature treatment of C_n@SWCNT systems ($T \sim 1500$ K) results in DWCNTs, offering higher thermal and chemical stability.[35] While, to our knowledge, the characterization of DWCNTs obtained by heating C_{80} peapods has not been reported yet, DWCNTs resulting from C_{60}@SWCNT and C_{70}@SWCNT peapods have been compared recently.[33] Although it was concluded that the resulting DWCNTs are not distinguishable, it was argued that molecular reorientations are required for the coalescence of neighboring fullerene molecules into an inner SWCNT. Our calculations therefore suggest a minimum tube radius for DWCNT formation from a C_{80} peapod larger than the radius required for C_{80} peapod encapsulation (at least larger than $R_1 \approx 6.95$ Å but arguably larger than $R_2 \approx 7.6$ Å, the radius required for the development of standing orientations). Note that, in this respect, it will be useful to carry out Monte Carlo simulations for a system consisting of several C_{80} molecules inside a SWCNT, and examine the thermal stability of the orientations observed in the present work.

The approximation of a continuous tube, i.e., neglecting the honeycomb network structure of the rolled-up graphene sheet, simplifies the energy calculations. Comparisons of Mercator maps obtained with and without this approximation confirm its validity, as for C_{60} (Ref. 9) and C_{70} (Ref. 10) peapods. For on-axis molecular configurations an expansion into SARFs can be elaborated; this significantly reduces the computation time. Using SARFs also helps one to appreciate the consequences of the D_{5d} symmetry on the nanotube's energy field and to understand the weak γ dependence seen in (β,γ) Mercator plots of the nanotube field. Note that when a belt of ten atoms is added to the middle of the C_{80} molecule, a tubular C_{90} molecule with D_{5h} symmetry results (similar to addition of a belt of ten C atoms to a C_{60} molecule resulting in a D_{5h} C_{70} molecule, and addition to a D_{5h} C_{70} molecule resulting in a D_{5d} C_{80} molecule; see Fig. 1). Continuation of this process would lead to C_{100},C_{110}, . . . molecules with alternating D_{5d},D_{5h}, . . . symmetry. The present extension of the SARF method to D_{5d} symmetry, together with the previous analysis of C_{70} molecules with D_{5h} symmetry,[10] therefore provides the complete analytical framework for nanotube field calculations for tubular fullerenes.

A realistic description of the arrangement of a fullerene molecule in a nanotube has to take into account the possibility of off-axis positions. We have found that from $R_3 \approx 8.00$ Å onward, the lowest energy no longer corresponds to an on-axis standing configuration, but to a lying orientation with the molecule "sticking" closer to the tube wall [Fig. 7(d)]. Again, this is obvious *a priori*, but our calculation provides a precise value for R_3. Interestingly, there is no regime where a standing off-axis configuration is favored. Upon comparing C_{80} and C_{70} peapods, we see that R_3 is larger for the former than for the latter ($R_3 \approx 7.6$ Å). On the other hand, the radius interval $[R_2,R_3]$ in which the standing orientation is realized is smaller for C_{80}@SWCNT than for C_{70}@SWCNT. Note that a standing configuration can be viewed as a sticking of the molecule to the tube wall as well: the two cap regions of the C_{80} molecule are both nearer to the tube and minimize the interaction energy. It will be interesting to examine whether a stable standing configuration can be obtained for the still larger tubular fullerenes C_n,$n = 90,100,110, \ldots$, mentioned above. Indeed, for these molecules, the molecule-tube interaction area can be increased by adopting an off-axis lying alignment [Fig. 7(d)], which might be energetically more favorable than the on-axis standing configuration [Fig. 7(c)]. We therefore argue that our present findings suggest that D_{5d} C_{80} molecules provide the ideal radius-dependent molecular orientational and positional behavior required for the design of orientation-induced tunable electronic functioning.

ACKNOWLEDGMENTS

The author gratefully acknowledges discussions with A. V. Nikolaev and K. H. Michel. This work was financially supported by the Research Foundation–Flanders (FWO-Vl).

APPENDIX: EXPANSION INTO SYMMETRY-ADAPTED ROTATOR FUNCTIONS

Here we briefly define the quantities entering Eqs. (2.6) and (2.7). For an intuitive derivation of the expansion into SARFs, we refer to Ref. 10.

The coefficients $\alpha_l^{\mathrm{t},n}(\lambda_\mathrm{t})$ are defined as

$$\alpha_l^{\mathrm{t},n}(\lambda_\mathrm{t}) = \frac{c_l^{\mathrm{t},n}(\lambda_\mathrm{t})}{g_l^{\mathrm{t}}(\lambda_\mathrm{t})}, \tag{A1}$$

with

$$c_l^{\mathrm{t},n}(\lambda_\mathrm{t}) = \sum_{\nu_\mathrm{t}} Y_l^n\left(\theta_{\lambda_\mathrm{t},\nu_\mathrm{t}},\phi_{\lambda_\mathrm{t},\nu_\mathrm{t}}\right), \tag{A2a}$$

$$g_l^{\mathrm{t}}(\lambda_\mathrm{t}) = \sqrt{\sum_{n=-l}^{l}\left[c_l^{\mathrm{t},n}(\lambda_\mathrm{t})\right]^2}. \tag{A2b}$$

Here, all ICs of a given type t (t = a,D,I) are grouped into layers with the same z- coordinate. The index ν_t labels the ICs within a layer; the index λ_t labels the layers. In Eq. (A2a), the Bradley-Cracknell spherical harmonics $Y_l^n(\theta,\phi)$ are understood,[25] and the spherical coordinates of the ICs are related to the Cartesian coordinates via $x_{\Lambda_\mathrm{t}} = r_{\Lambda_\mathrm{t}}\sin\theta_{\Lambda_\mathrm{t}}\cos\phi_{\Lambda_\mathrm{t}}$, $y_{\Lambda_\mathrm{t}} = r_{\Lambda_\mathrm{t}}\sin\theta_{\Lambda_\mathrm{t}}\sin\phi_{\Lambda_\mathrm{t}}$, $z_{\Lambda_\mathrm{t}} = r_{\Lambda_\mathrm{t}}\cos\theta_{\Lambda_\mathrm{t}}$.

The coefficients $\alpha_l^{\mathrm{t},n}(\lambda_\mathrm{t})$ obey the selection rule [Eq. (2.9)] for D_{5d} symmetry.

The coefficients $w_l^{\mathrm{t}}(\lambda_\mathrm{t},R)$ are defined as follows:

$$w_l^{\mathrm{t}}(\lambda_\mathrm{t},R) = g_l^{\mathrm{t}}(\lambda_\mathrm{t})\tilde{v}_l^{\mathrm{t}}(R,\lambda_\mathrm{t}), \tag{A3a}$$

$$\tilde{v}_l^{\mathrm{t}}(R,\lambda_\mathrm{t}) = 2\pi\int_0^{2\pi} d\Phi\int_{-\infty}^{+\infty} dZ\int_0^{\pi}\sin\theta\, d\theta\ \tilde{v}^{\mathrm{t}} \times\left(R,r_{\lambda_\mathrm{t}},\theta_{\lambda_\mathrm{t}},\Phi,Z\right)Y_l^{m=0}(\cos\theta), \tag{A3b}$$

where $\tilde{v}_l^{\mathrm{t}}(R,r_{\lambda_\mathrm{t}},\Phi,Z) = v^{\mathrm{t}}(|\vec{\rho}-\vec{r}_{\Lambda_\mathrm{t}}|)$ stands for the evaluation of the interaction potential at the distance

$$\left|\vec{\rho}-\vec{r}_{\Lambda_\mathrm{t}}\right| = \left\{R^2 + r_{\Lambda_\mathrm{t}}^2\sin^2\theta_{\Lambda_\mathrm{t}} - 2Rr_{\Lambda_\mathrm{t}}\cos(\Phi-\phi_{\Lambda_\mathrm{t}})\sin\theta_{\Lambda_\mathrm{t}} + Z^2 + r_{\Lambda_\mathrm{t}}^2\cos^2\theta_{\Lambda_\mathrm{t}} - 2Zr_{\Lambda_\mathrm{t}}\cos\theta_{\Lambda_\mathrm{t}}\right\}^{\frac{1}{2}}. \tag{A4}$$

Here, $\vec{\rho} = (R,\Phi,Z)$ and $\vec{r}_{\lambda_\mathrm{t}} = (r_{\lambda_\mathrm{t}},\theta_{\lambda_\mathrm{t}},\phi_{\lambda_\mathrm{t}})$ stand for the coordinate vectors of a point on the nanotube and of the IC, in cylindrical and spherical coordinates, respectively.

[1] B. W. Smith, M. Monthioux, and D. E. Luzzi, Nature (London) **396**, 323 (1998).

[2] H. Kataura, Y. Maniwa, T. Kodama, K. Kikuchi, K. Hirahara, K. Suenaga, S. Iijima, S. Suzuki, Y. Achiba, and W. Krätschmer, Synth. Met. **121**, 1195 (2001).

[3] K. Hirahara, S. Bandow, K. Suenaga, H. Kato, T. Okazaki, H. Shinohara, and S. Iijima, Phys. Rev. B **64**, 115420 (2001).

[4] S. Bandow, M. Takizawa, H. Kato, T. Okazaki, H. Shinohara, and S. Iijima, Chem. Phys. Lett. **347**, 23 (2001).

[5] J. Sloan, A. I. Kirkland, J. L. Hutchison, and M. L. H. Green, Chem. Commun. **2002**, 1319 (2002).

[6] O. Vostrowsky and A. Hirsch, Angew. Chem., Int. Ed. Engl. **43**, 2326 (2004).

[7] M. Monthioux, E. Flahaut, and J.-P. Cleuziou, J. Mater. Res. **21**, 2774 (2006).

[8] R. Kitaura and H. Shinohara, Chem. Asian J. **1**, 646 (2006).

[9] B. Verberck and K. H. Michel, Phys. Rev. B. **74**, 045421 (2006).

[10] B. Verberck and K. H. Michel, Phys. Rev. B **75**, 045419 (2007).

[11] B. Verberck and K. H. Michel, Int. J. Quantum Chem. **107**, 2294 (2007).

[12] K. H. Michel, B. Verberck, and A. V. Nikolaev, Phys. Rev. Lett. **95**, 185506 (2005).

[13] K. H. Michel, B. Verberck, and A. V. Nikolaev, Eur. Phys. J. B **48**, 113 (2005).

[14] S. Rols, J. Cambedouzou, M. Chorro, H. Schober, V. Agafonov, P. Launois, V. Davydov, A. V. Rakhmanina, H. Kataura, and J.-L. Sauvajol, Phys. Rev. Lett. **101**, 065507 (2008).

[15] A. N. Khlobystov, R. Scipioni, D. Nguyen-Manh, D. A. Britz, D. G. Pettifor, G. A. D. Briggs, S. G. Lyapin, A. Ardavan, and R. J. Nicholas, Appl. Phys. Lett. **84**, 792 (2004).

[16] L. Guan, H. Li, Z. Shi, L. You, and Z. Gu, Solid State Commun. **133**, 333 (2005).

[17] M. Chorro, A. Delhey, L. Noé, M. Monthioux, and P. Launois, Phys. Rev. B **75**, 035416 (2007).

[18] S. Okubo, T. Okazaki, K. Hirose-Takai, K. Suenaga, S. Okada, S. Bandow, and S. Iijima, J. Am. Chem. Soc. **132**, 15252 (2010).

[19] Y. Sato, K. Suenaga, S. Okubo, T. Okazaki, and S. Iijima, Nano Lett. **7**, 3704 (2007).

[20] Several isomers of C_{80} fulfilling the isolated-pentagon rule can be conceived, with I_h, D_{5h}, D_{5d}, D_3, D_2, and C_{2v} symmetry (Ref. 21). In this work, we consider the D_{5d} C_{80} isomer reported in Ref. 22. The C_{80} peapods studied in Ref. 19 were synthesized from D_{5d} C_{80} molecules. Throughout the paper, we use the shorthand notation C_{80} for D_{5d} C_{80}.

[21] P. W. Fowler and D. E. Manolopoulos, *An Atlas of Fullerenes* (Oxford University Press, Oxford, 1995).

[22] C.-R. Wang, T. Sugai, T. Kai, T. Tomiyama, and H. Shinohara, Chem. Commun. **2000**, 557 (2000).

[23] The transformation reads $\phi(t) = \mathrm{TAN}^{-1}[y(t)/x(t)]$, $\theta(t) = \cos^{-1}[z(t)/\sqrt{x(t)^2+y(t)^2+z(t)^2}]$, where $\mathrm{TAN}^{-1}(y/x) = \tan^{-1}(y/x)$ if $x \geqslant 0$ and $\tan^{-1}(y/x)+\pi$ if $x < 0$.

[24] Named after Gerardus Mercator (1512–1594), Flemish cartographer, inventor of the cylindrical projection. The angles θ and ϕ correspond to geographical latitude and longitude, respectively.

[25] C. J. Bradley and A. P. Cracknell, *The Mathematical Theory of Symmetry in Solids* (Clarendon, Oxford, 1972).

[26] [http://www.cochem2.tutkie.tut.ac.jp/Fuller/higher/higherE.html].

[27] R. Saito, G. Dresselhaus, and M. S. Dresselhaus, *Physical Properties of Carbon Nanotubes* (Imperial College Press, London, 1998).

[28] N. Hamada, S. Sawada, and A. Oshiyama, Phys. Rev. Lett. **68**, 1579 (1992); D. H. Robertson, D. W. Brenner, and J. W. Mintmire, Phys. Rev. B **45**, 12592 (1992).

[29] P. Launois, S. Ravy, and R. Moret, Phys. Rev. B **55**, 2651 (1997).

[30] D. Lamoen and K. H. Michel, J. Chem. Phys. **101**, 1435 (1994).

[31] A. K. Callebaut and K. H. Michel, Phys. Rev. B **52**, 15279 (1995).

[32] These results coincide with the calculations of Ref. 10 [Fig. 8b therein], but for the purpose of this paper we have (re)calculated them for a larger range of tube radii.

[33] P. Launois, M. Chorro, B. Verberck, P.-A. Albouy, S. Rouzière, D. Colson, A. Forget, L. Noé, H. Kataura, M. Monthioux, and J. Cambedouzou, Carbon **48**, 89 (2010).

[34] B. Verberck, J. Cambedouzou, G. A. Vliegenthart, G. Gompper, and P. Launois (accepted for publication in Carbon).

[35] For a review, see R. Pfeiffer, T. Pichler, Y. A. Kim, and H. Kuzmany, Top. Appl. Phys. **111**, 495 (2008).